www.oncotarget.com Oncotarget, 2024, Vol. 15, pp: 159-174

Research Paper

GZ17-6.02 interacts with proteasome inhibitors to kill multiple myeloma cells

Laurence Booth[1], Jane L. Roberts[1], Cameron West[2] and Paul Dent[1]

[1]Department of Biochemistry and Molecular Biology, Virginia Commonwealth University, Richmond, VA 23298, USA

[2]Genzada Pharmaceuticals, Hutchinson, KS 67502, USA

Correspondence to: *Paul Dent*, ***email***: *paul.dent@vcuhealth.org*

Keywords: autophagy; ER stress; GZ17-6.02; bortezomib; proteasome inhibitor

Received: *December 01, 2023* ***Accepted***: *January 23, 2024* ***Published***: *March 05, 2024*

ABSTRACT

GZ17-6.02, a synthetically manufactured compound containing isovanillin, harmine and curcumin, has undergone phase I evaluation in patients with solid tumors (NCT03775525) with a recommended phase 2 dose (RP2D) of 375 mg PO BID. GZ17-6.02 was more efficacious as a single agent at killing multiple myeloma cells than had previously been observed in solid tumor cell types. GZ17-6.02 interacted with proteasome inhibitors in a greater than additive fashion to kill myeloma cells and alone it killed inhibitor-resistant cells to a similar extent. The drug combination of GZ17-6.02 and bortezomib activated ATM, the AMPK and PERK and inactivated ULK1, mTORC1, eIF2α, NFκB and the Hippo pathway. The combination increased ATG13 S318 phosphorylation and the expression of Beclin1, ATG5, BAK and BIM, and reduced the levels of BCL-XL and MCL1. GZ17-6.02 interacted with bortezomib to enhance autophagosome formation and autophagic flux, and knock down of ATM, AMPKα, ULK1, Beclin1 or ATG5 significantly reduced both autophagy and tumor cell killing. Knock down of BAK and BIM significantly reduced tumor cell killing. The expression of HDACs1/2/3 was significantly reduced beyond that previously observed in solid tumor cells and required autophagy. This was associated with increased acetylation and methylation of histone H3. Combined knock down of HDACs1/2/3 caused activation of ATM and the AMPK and caused inactivation of ULK1, mTORC1, NFκB and the Hippo pathway. HDAC knock down also enhanced ATG13 phosphorylation, increased BAK levels and reduced those of BCL-XL. Collectively, our present studies support performing additional *in vivo* studies with multiple myeloma cells.

INTRODUCTION

Multiple myeloma (MM) is a clonal disorder of plasma cells accounting for 13% of hematologic malignancies; ~35,000 patients per annum are diagnosed in the USA, with the disease more common in males [1–3]. Despite advances in the treatment of MM over the past 10–15 years with the introduction of proteasome inhibitors, e.g., bortezomib (Velcade, BTZ) and subsequently carfilzomib (Kyprolis) and ixazomib (Ninlaro), and more recently with immunomodulatory approaches and antibodies, the median life expectancy of MM patients remains sub-optimal at ~7–8 years [4–6]. However, not all myeloma patients respond to proteasome inhibitors and myeloma cells can evolve under this selective proteasome inhibitor pressure to become drug-resistant.

More recently, the myeloma therapeutics field has been dramatically altered by the use of CAR-T cells and other immunotherapeutics. [7–10]. Two CAR-T cells products, directed against the Anti-B-cell maturation antigen (BCMA), idecabtagene vicleucel (ide-cel) and ciltacabtagene autoleucel (cilta-cel), have recently received FDA approval for relapsed/refractory MM in patients who had already underwent four or more prior lines of therapy. Response rates of up to ~90% have been observed in patients who were otherwise untreatable.

However, it has also been noted that CAR T-cell therapies are often associated with immune system adverse events, for example, cytokine release syndrome, various cytopenias, and infections. Some patients treated with CAR-T cells can also relapse after treatment. Collectively, this implies that there remains a patient population that could benefit from novel therapeutic approaches using GZ17-6.02.

The novel therapeutic agent GZ17-6.02 (602) is comprised of three synthetically manufactured natural compounds in the following ratio: isovanillin (77%), harmine (13%) and curcumin (10%) [11]. Curcumin as a single agent has low solubility in water, has very poor PK/PD *in vivo* and failed in the clinic as an anti-cancer agent [12, 13]. In our prior *in vitro* studies using low physiologic concentrations of curcumin, the generation of reactive oxygen species played an important role in the process by which tumor cells were killed [14]. However, the anti-tumor biology of curcumin when combined with isovanillin and harmine is different to that of free curcumin, apparently requiring minimal, if any, ROS generation [15–23].

Harmine is isolated from the plants *Arum palaestinum* and *Peganum harmala* and like curcumin, has been used as a medicinal herb for millennia [24–26]. Prior work has argued that harmine selectively kills tumor cells over normal tissues. Harmine can cause DNA damage and has been reported to inhibit drug efflux pumps. Isovanillin is an isomer of vanillin, isolated from the vanilla bean, and is an inhibitor of aldehyde oxidase and xanthine oxidase. It can donate a proton forming a hydrogen bond and accept three hydrogen bonds from other compounds [27–29]. Combined with our curcumin findings, we believe that isovanillin can complex with curcumin and harmine to create an entity with unique biology when compared to the three individual agents [14].

GZ17-6.02 received its IND in 2018 from the FDA and has undergone phase I evaluation in patients with solid tumors (NCT03775525). The RP2D is 375 mg PO BID. In the trial a PR was observed in a c-MET amplified NSCLC, a prolonged SD with 20% tumor shrinkage in a HER2 mutant NSCLC, and prolonged SD responses in multiple other tumor types, including the almost untreatable disease, uveal melanoma. The safety profile of the drug was outwardly benign in patients with only grade 1/2/3 reversible alterations in plasma liver enzyme levels. Laboratory-based PK/PD studies with the drug have shown that all three components of GZ17-6.02 were concentrated in tumors at concentrations above those used for our *in vitro* studies. In colorectal and prostate tumors GZ17-6.02 as a single agent significantly prolonged animal survival beyond the drug-treatment time-frame. We believe that developing GZ17-6.02 as a novel MM agent potentially opens up a multitude of novel opportunities to develop therapeutic approaches which will prolong patient survival.

RESULTS

Our first series of studies defined the interactions of the individual components of GZ17-6.02 in multiple myeloma cells. As single agents, only curcumin caused substantial significant cell killing 48 h after drug exposure (Figure 1A). The dual combination of harmine and isovanillin exhibited almost no further activity compared to harmine alone, which was similar to the combinations of curcumin with either agent to curcumin alone. In contrast, GZ17-6.02 which contains all three agents caused significantly greater levels of tumor cell killing than would be predicted based on the effects of the three individual components [14]. We next determined whether GZ17-6.02 interacted with proteasome inhibitors to kill MM cells. GZ17-6.02 interacted in a greater-than-additive fashion with both bortezomib and carfilzomib to kill MM cells 24 h after drug exposure (Figure 1B).

The data presented in Figure 1B with GZ17-6.02 as a single agent piqued our interest as we were observing ~20% tumor cell killing, which appeared to be higher than we previously reported in solid tumor cells. Hence, we made direct comparisons between the lethality of GZ17-6.02 in MM cells, prostate cancer cells and NSCLC cells. GZ17-6.02 was significantly more efficacious at killing MM cells when compared to prostate and lung cancer cells (Supplementary Figure 1). This is also of particular translational interest as we recently demonstrated that GZ17-6.02 as a single agent significantly prolonged survival in a mouse model of prostate cancer [17].

A key mechanism mediating GZ17-6.02 lethality in solid tumor cells is by enhancing macroautophagy [15–23]. Both GZ17-6.02 and bortezomib enhanced the formation of autophagosomes in MM cells and interacted together to promote additional vesicle formation (Figure 2). Over time, the number of autophagosomes declined and the numbers of autolysosomes increased, indicative that we were also observing autophagic flux. In an identical fashion to our comparative studies in Supplementary Figure 1, we compared the ability of GZ17-6.02 to increase the formation of autophagosomes and autolysosomes in both liquid and solid tumor cell types (Supplementary Figure 2). GZ17-6.02 was significantly more capable of increasing autophagosome levels in MM cells than in prostate cancer cells. When we determined the subsequent formation of autolysosomes, however, there was no significant obvious difference between the two tumor cell types. MM cells made resistant to BTZ were killed by GZ17-6.02 in a similar manner to parental sensitive cells, however, the interaction between GZ17-6.02 and BTZ was considerably reduced (Figure 3).

We determined the impact GZ17-6.02 had on cell signaling processes in the MM cells. The drug combination of GZ17-6.02 and bortezomib in MM cells activated ATM, the AMPK and PERK and inactivated ULK1, mTORC1, eIF2α, NFκB and the Hippo pathway (Figures 4A, 4B and 5A, 5B; Supplementary Figure 3A, 3B). The drug combination increased ATG13 S318 phosphorylation and the expression of Beclin1, ATG5, BAK and BIM, and reduced the levels of BCL-XL and MCL1. Collectively, these alterations would predict for enhance tumor cell death. GZ17-6.02 interacted with bortezomib to enhance autophagosome formation and autophagic flux, and knock down of ATM, AMPKα, ULK1, Beclin1 or ATG5 significantly reduced both autophagy and tumor cell killing (Figure 6 and Supplementary Figure 4). This data, with respect to the findings in Supplementary Figure 2, also suggests that in multiple myeloma cells autophagosome formation caused by GZ17-6.02 initiates a

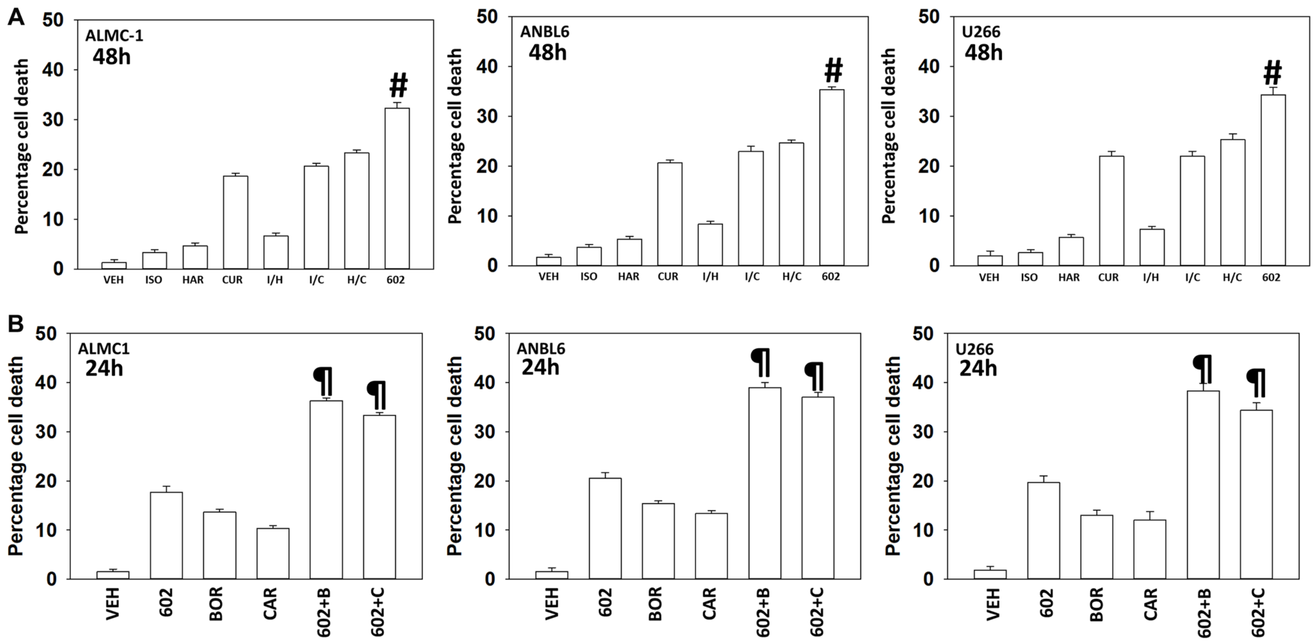

Figure 1: GZ17-6.02 and proteasome inhibitors interact in a greater than additive fashion to kill multiple myeloma cells. (**A**) ALMC1, ANBL6 and U266 cells were treated with vehicle control, GZ17-6.02 (curcumin (2.0 μM) + harmine (4.5 μM) + isovanillin (37.2 μM)) or with component parts of GZ17-6.02 as individual agents at the indicated concentrations or in duo combinations. Cells were isolated 48 h afterwards and viability determined via trypan blue exclusion assays (n = 3 +/− SD). $^{\#}p < 0.05$ greater than other tested drug treatments. (**B**) ALMC1, ANBL6 and U266 cells were treated with vehicle control, GZ17-6.02 (2 μM curcumin, final), bortezomib (10 nM), carfilzomib (5 nM) or the drugs in combination, as indicated. Twenty-four h later, cells were isolated, and viability determined via trypan blue exclusion assays (n = 3 +/− SD). $^{¶}p < 0.05$ greater than other tested drug treatments.

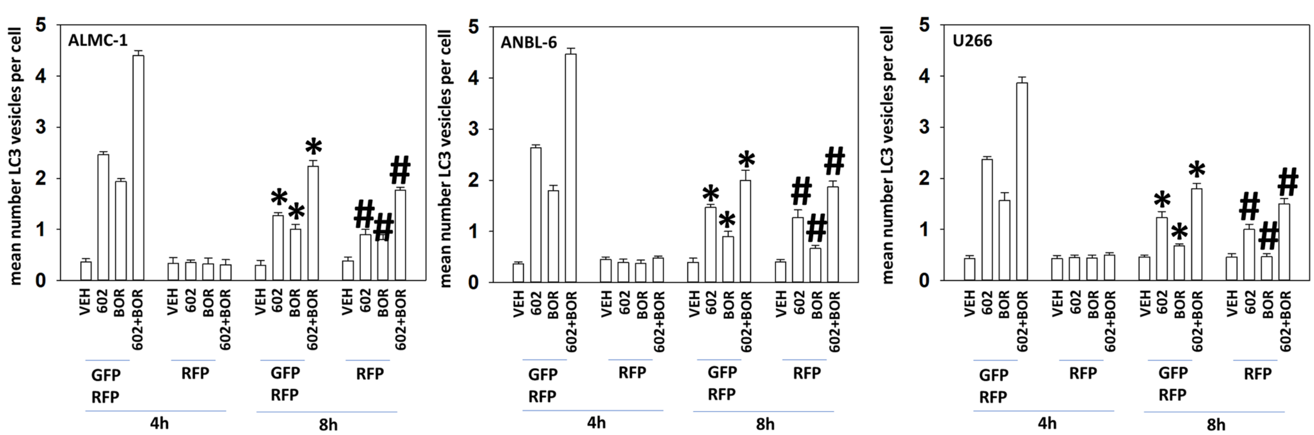

Figure 2: GZ17-6.02 and bortezomib interact to cause autophagosome formation and autophagic flux. ALMC1, ANBL6 and U266 cells were transfected with a plasmid to express LC3-GFP-RFP. Twenty-four h later, cells were treated with vehicle control, GZ17-6.02 (curcumin 2 μM, final), bortezomib (10 nM) or the drugs in combination for 4 h and 8 h. At each time point, the mean number of autophagosomes (GFP+ RFP+) and autolysosomes (RFP+) per cell were determined randomly in >100 cells. (n = 3 +/− SD). $^{*}p < 0.05$ less than corresponding value at 4 h; $^{\#}p < 0.05$ greater than corresponding value at 4 h.

pathway towards cell death that does not per se involve the formation of autolysosomes and autophagic flux. Knock down of eIF2α, BAK, BIM or CD95 significantly reduced tumor cell killing (Figure 7). Knock down of eIF2α or BAK exhibited the greatest cytoprotective effects against GZ17-6.02 as a single agent and when combined with bortezomib when compared to the knock down of other proteins.

The expression of HDACs1/2/3 was significantly reduced by GZ17-6.02 beyond that previously observed in prostate cancer cells and, this observation required macroautophagy (Figures 4A, 4B and 5A, 5B; Supplementary Figures 5 and 6) [15–23]. This was associated with changes in the acetylation, methylation, and phosphorylation of histone H3 at multiple NH_2-terminal regulatory sites (Figure 8A, 8B and Supplementary Figure 7). The acetylation of histone H3 at K9 and K27 was enhanced by the drug combination after 4 h, and this was maintained for 48 h, even in cells that had spent 24 h in the absence of drugs. Changes in histone H3 methylation were observed after 24 h and 48 h, with methylation levels both increasing and decreasing. After 24 h, in both lines, the di-methylation of histone H3 K4 was enhanced and the mono-methylation of K36 and K79 declined. After 48 h, the di-methylation of K4 remained elevated and the di-methylation of K27 was also increased. The methylation of K79 remained lower.

GZ17-6.02 also increased the phosphorylation of histone H3. The phosphorylation of histone H3 T3 observed after 4 h and was maintained over the 48 h time course. The phosphorylation of histone H3 S10 was elevated after 4 h, but then declined in ALMC1 cells whereas it was maintained in ANBL6 cells. The phosphorylation of histone H3 S28 was transiently enhanced after 24 h only in ALMC1 cells. The phosphorylation of histone H3 T11 was unaltered at any time point in either line.

Combined knock down of HDACs1/2/3 caused activation of ATM and the AMPK and caused inactivation of ULK1, mTORC1, NFκB and the Hippo pathway (Figures 9A, 9B and 10A, 10B). HDAC knock down also enhanced ATG13 S318 phosphorylation, i.e., autophagosome formation, increased BAK levels and reduced those of BCL-XL, although it did not enhance endoplasmic reticulum stress signaling as judged by eIF2α S51 phosphorylation. Thus, GZ17-6.02 initially causes a series of signaling events which leads to autophagic degradation of HDACs 1, 2 and 3, which then directly induces, as a secondary event, many of the same alterations in cell signaling within the multiple myeloma cells caused by GZ17-6.02, ultimately causing tumor cell death.

DISCUSSION

We recently demonstrated that GZ17-6.02 was highly efficacious at suppressing the growth of LNCaP prostate tumors in mice, significantly prolonging survival weeks beyond the cessation of drug exposure [21]. The present studies were performed to extend our knowledge of GZ17-6.02 biology from that known in solid tumor cell types such as prostate cancer cells to liquid tumor cell types, for example, multiple myeloma. Many of the biological processes engaged by GZ17-6.02 in solid tumor cells were also found to operate in MM cells, however, there were also notable differences. For example, the ability of GZ17-6.02 to reduce the expression of HDACs1/2/3 was enhanced in the MM cells compared to solid tumor cells whereas the degradation of HDAC6 was reduced. GZ17-6.02 promoted greater levels of autophagosome formation in MM cells compared to solid tumor cell types, but the amount of autophagic flux to autolysosomes was not significantly enhanced. GZ17-6.02 was significantly better at killing MM cells than prostate cancer cells, and in both tumor types, knock down of ULK1, Beclin1 or ATG5 reduced both autophagosome formation and tumor cell killing.

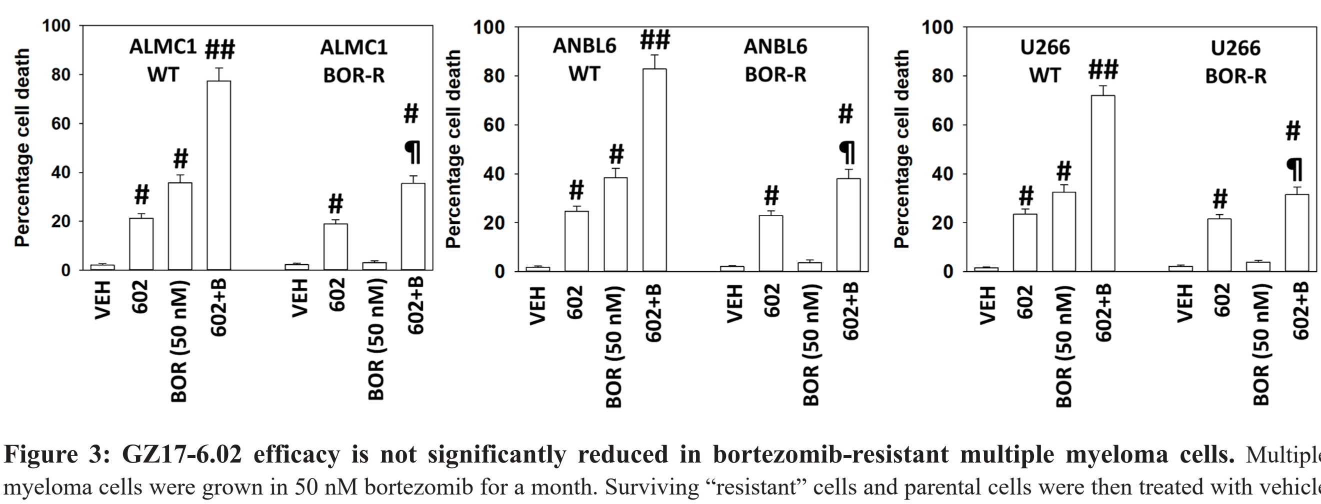

Figure 3: GZ17-6.02 efficacy is not significantly reduced in bortezomib-resistant multiple myeloma cells. Multiple myeloma cells were grown in 50 nM bortezomib for a month. Surviving "resistant" cells and parental cells were then treated with vehicle control, GZ17-6.02 (2 µM curcumin, final), bortezomib (50 nM) or the drugs in combination for 24 h. Cells were isolated after 24 h and viability determined by trypan blue exclusion assay ($n = 3$ +/− SD) $^{\#}p < 0.05$ greater than vehicle control; $^{\#\#}p < 0.05$ greater than GZ17-6.02 single agent value; $^{¶}p < 0.05$ less than corresponding value in wild type parental cells.

Multiple myeloma cells made resistant to bortezomib remained sensitive to being killed by GZ17-6.02 with no significant difference comparing parental and resistant cells. The reasons for this observation are presently unclear, in part, because the studies in our initial report have been focused on developing an initial understanding

A ALMC1 4h

	VEH	602	BTZ	602+B
ATM	100	100	102	100
P-ATM S1981	100	107	114#	117#
AMPKα	100	100	100	99
P-AMPKα T172	100	110	109	115#
mTOR	100	100	102	102
P-mTOR S2448	100	92	92	86*
P-mTOR S2481	100	93	94	91
ULK1	100	99	99	99
P-ULK1 S757	100	87*	81*	78*
P-ULK1 S317	100	102	104	104
eIF2α	100	100	99	101
P-eIF2α S51	100	111	109	117#
PERK	100	98	99	101
P-PERK T980	100	114#	106	117#

	VEH	602	BTZ	602+B
AKT	100	100	101	100
P-AKT T308	100	91	95	89
STAT3	100	99	109	99
P-STAT3 Y705	100	89	105	91
STAT5	100	99	105	97
P-STAT5 Y694	100	91	106	96
Beclin1	100	111	111	118#
ATG5	100	108	109	113#
ATG13	100	103	101	100
P-ATG13 S318	100	112	109	115#
GRP78	100	105	104	108
CHOP	100	97	106	106
PP1	100	98	101	103

	VEH	602	BTZ	602+B
NFκB	100	100	101	100
P-NFκB S536	100	93	92	86*
c-SRC	100	100	100	100
P-SRC Y416	100	90	92	83*
P-SRC Y527	100	108	102	110
c-MET	100	98	100	99
P-c-MET	100	89	85*	84*
CD95	100	102	104	104
FAS-L	100	108	108	111
JAK2	100	99	104	101
P-JAK2	100	99	103	98
c-KIT	100	97	102	98
P-c-KIT	100	99	103	92
p70 S6K	100	100	100	99
P-p70 S6K T389	100	89	94	85*
JNK1/2	100	98	99	100
P-JNK1/2	100	104	110	115#
p38	100	99	98	99
P-p38	100	100	102	111
ERK1/2	100	100	99	100
P-ERK1/2	100	93	89	85*

B

	VEH	602	BTZ	602+B
HDAC1	100	78*	84*	72**
HDAC2	100	75*	77*	57**
HDAC3	100	74*	91	67**
HDAC4	100	96	98	97
HDAC5	100	100	100	92
HDAC6	100	90	95	85*
HDAC7	100	95	98	95
HDAC8	100	99	99	97
HDAC9	100	100	97	98
HDAC10	100	101	100	98
HDAC11	100	100	101	101
ERK2	100	100	100	100

	VEH	602	BTZ	602+B
LATS1/2	100	100	100	100
P-LATS T1097	100	118#	113#	124#
P-LATS S909	100	119#	118#	125#
YAP	100	100	99	98
P-YAP S109	100	106	102	116#
P-YAP S127	100	113#	106	118#
P-YAP S397	100	114#	111	117#
TAZ	100	100	100	100
P-TAZ S89	100	109	104	119#
ERK2	100	100	100	100

	VEH	602	BTZ	602+B
PD-L1	100	88	97	84*
PD-L2	100	98	99	97
MHCA	100	112	104	114#
ODC	100	98	101	99
IDO1	100	98	100	95
p38 MAPK	100	100	99	99
P-p38	100	101	99	110
BCL-XL	100	86*	95	82*
MCL1	100	88	92	86*
BAX	100	99	101	99
BAK	100	111	104	118#
BIM	100	108	107	115#
FLIP-s	100	93	94	86*
ERK2	100	100	100	100

Figure 4: (**A**) GZ17-6.02 and bortezomib regulate signaling pathways in ALMC1 cells. Cells were treated with vehicle control, GZ17-6.02 (2 µM, curcumin final), bortezomib (10 nM) or the drugs in combination for 4 h. Cells were centrifuged and fixed *in situ*, permeabilized, stained with the indicated validated primary antibodies and imaged with secondary antibodies carrying red- and green-fluorescent tags. The staining intensity of at least 100 cells per well/condition is determined in three separate studies. The data are the normalized amount of fluorescence set at 100% comparing intensity values for vehicle control ($n = 3$ +/− SD). $^{\#}p < 0.05$ greater than vehicle control; $^{*}p < 0.05$ less than vehicle control. Tabular data are presented as a heat-map (Microsoft Excel: conditional formatting, color scales: green, yellow, red). Green indicates greater levels and red indicates lower levels of staining. (**B**) GZ17-6.02 and bortezomib regulate signaling pathways in ALMC1 cells. Cells were treated with vehicle control, GZ17-6.02 (2 µM, curcumin final), bortezomib (10 nM) or the drugs in combination for 4 h. Cells were centrifuged and fixed *in situ*, permeabilized, stained with the indicated validated primary antibodies and imaged with secondary antibodies carrying red- and green-fluorescent tags. The staining intensity of at least 100 cells per well/condition is determined in three separate studies. The data are the normalized amount of fluorescence set at 100% comparing intensity values for vehicle control ($n = 3$ +/− SD). $^{\#}p < 0.05$ greater than vehicle control; $^{*}p < 0.05$ less than vehicle control. Tabular data are presented as a heat-map (Microsoft Excel: conditional formatting, color scales: green, yellow, red). Green indicates greater levels and red indicates lower levels of staining.

of GZ17-6.02 biology in parental cells and its interaction with bortezomib. Several publications have argued that bortezomib-induced autophagy acts to reduce drug efficacy [30–34]. Other groups, however, state that drug-induced autophagy results in MM cell apoptosis [35, 36]. Our data demonstrated that GZ17-6.02 and bortezomib

A ANBL6 4h

	VEH	602	BTZ	602+B
ATM	100	100	99	99
P-ATM S1981	100	112	116#	122#
AMPKα	100	100	100	99
P-AMPKα T172	100	111	111	116#
mTOR	100	100	99	100
P-mTOR S2448	100	91	89	84*
P-mTOR S2481	100	91	92	91
ULK1	100	100	99	100
P-ULK1 S757	100	94	90	82*
P-ULK1 S317	100	107	105	109
eIF2α	100	100	100	99
P-eIF2α S51	100	111	107	117#
PERK	100	99	99	100
P-PERK T980	100	108	108	114#

ANBL6 4h

	VEH	602	BTZ	602+B
AKT	100	101	100	100
P-AKT T308	100	91	94	86*
STAT3	100	100	100	100
P-STAT3 Y705	100	90	92	85*
STAT5	100	100	99	98
P-STAT5 Y694	100	90	90	85*
Beclin1	100	110	103	116#
ATG5	100	108	107	113#
ATG13	100	101	100	100
P-ATG13 S318	100	106	104	121#
GRP78	100	107	106	107
CHOP	100	103	103	113#
PP1	100	100	105	105

	VEH	602	BTZ	602+B
NFκB	100	99	99	100
P-NFκB S536	100	90	87*	82*
c-SRC	100	99	99	100
P-SRC Y416	100	90	95	85*
P-SRC Y527	100	104	101	114#
c-MET	100	102	100	100
P-c-MET	100	93	91	86*
CD95	100	99	100	100
FAS-L	100	107	106	113#
JAK2	100	100	100	101
P-JAK2	100	101	101	100
c-KIT	100	99	99	99
P-c-KIT	100	101	88	84*
p70 S6K	100	99	100	99
P-p70 S6K T389	100	93	89	86*
JNK1/2	100	101	99	100
P-JNK1/2	100	97	95	93
p38	100	100	99	98
P-p38	100	100	102	102
P-ERK1/2	100	98	115#	103
ERK1/2	100	100	99	99

B

	VEH	602	BTZ	602+B
HDAC1	100	81*	88	77*
HDAC2	100	84*	80*	66**
HDAC3	100	81*	92	73**
HDAC4	100	99	101	99
HDAC5	100	100	101	98
HDAC6	100	90	95	87*
HDAC7	100	98	99	98
HDAC8	100	100	100	98
HDAC9	100	98	98	98
HDAC10	100	100	100	100
HDAC11	100	100	99	100
ERK2	100	100	99	100

	VEH	602	BTZ	602+B
LATS1/2	100	100	101	101
P-LATS T1097	100	110	105	117#
P-LATS S909	100	111	114#	117#
YAP	100	99	99	100
P-YAP S109	100	108	105	108
P-YAP S127	100	114#	114#	117#
P-YAP S397	100	113#	113#	117#
TAZ	100	100	101	101
P-TAZ S89	100	111	108	121#
ERK2	100	100	101	99

	VEH	602	BTZ	602+B
PD-L1	100	87*	98	87*
PD-L2	100	100	101	99
MHCA	100	117#	103	117#
ODC	100	101	100	101
IDO1	100	97	98	94
p38 MAPK	100	99	101	99
P-p38	100	99	99	108
BCL-XL	100	90	96	85*
MCL1	100	93	98	84*
BAX	100	98	101	100
BAK	100	115#	114#	124#
BIM	100	115#	111	125#
FLIP-s	100	97	97	96
ERK2	100	100	100	100

Figure 5: (**A**) GZ17-6.02 and bortezomib regulate signaling pathways in ANBL6 cells. Cells were treated with vehicle control, GZ17-6.02 (2 μM, curcumin final), bortezomib (10 nM) or the drugs in combination for 4 h. Cells were centrifuged and fixed *in situ*, permeabilized, stained with the indicated validated primary antibodies and imaged with secondary antibodies carrying red- and green-fluorescent tags. The staining intensity of at least 100 cells per well/condition is determined in three separate studies. The data are the normalized amount of fluorescence set at 100% comparing intensity values for vehicle control (n = 3 +/− SD). $^{\#}p < 0.05$ greater than vehicle control; $^{*}p < 0.05$ less than vehicle control. Tabular data are presented as a heat-map (Microsoft Excel: conditional formatting, color scales: green, yellow, red). Green indicates greater levels and red indicates lower levels of staining. (**B**) GZ17-6.02 and bortezomib regulate signaling pathways in ANBL6 cells. Cells were treated with vehicle control, GZ17-6.02 (2 μM, curcumin final), bortezomib (10 nM) or the drugs in combination for 4 h. Cells were centrifuged and fixed *in situ*, permeabilized, stained with the indicated validated primary antibodies and imaged with secondary antibodies carrying red- and green-fluorescent tags. The staining intensity of at least 100 cells per well/condition is determined in three separate studies. The data are the normalized amount of fluorescence set at 100% comparing intensity values for vehicle control (n = 3 +/− SD). $^{\#}p < 0.05$ greater than vehicle control; $^{*}p < 0.05$ less than vehicle control. Tabular data are presented as a heat-map (Microsoft Excel: conditional formatting, color scales: green, yellow, red). Green indicates greater levels and red indicates lower levels of staining.

had similar overlapping mechanisms regulating cell killing, supporting the notion that autophagy feeds into apoptosis. Bortezomib-induced cell death was significantly reduced by knock down of ATM, AMPKα, ULK1, Beclin1 or ATG5, with all knock downs reducing the amount of killing to the same extent. In contrast for GZ17-6.02 as a single agent or when combined with bortezomib, a slightly different biology was observed. Knock down of ATM or AMPKα significantly reduced killing whereas knock down of ULK1, Beclin1 or ATG5 caused a further additional significant reduction in cell death. Unlike solid tumor cells where GZ17-6.02 as a single agent always was observed to cause significant amounts of ATM activation, this effect was not observed in MM cells, and unexpectedly, we found that bortezomib as a single agent activated ATM. Studies beyond the scope of this manuscript will be required to study bortezomib-induced ATM activation in parental cells and in bortezomib-resistant cells.

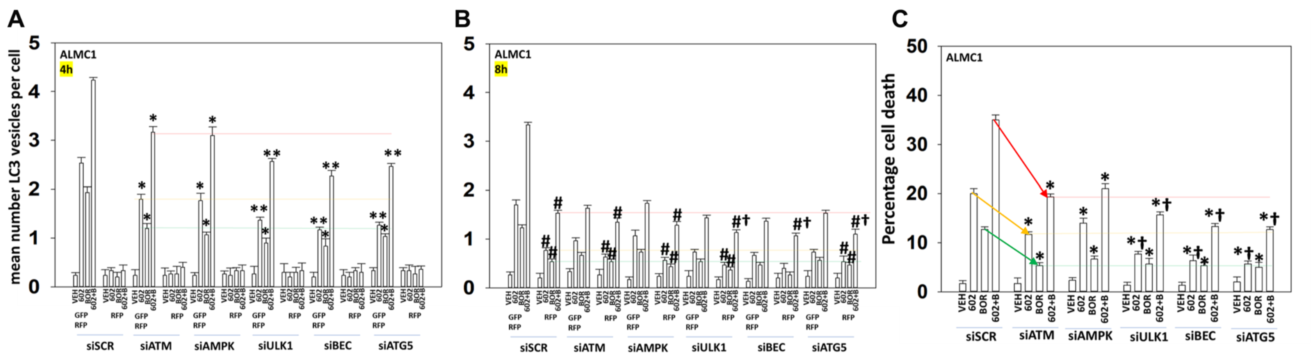

Figure 6: Signaling by ATM-AMPK and autophagosome formation are toxic events when cells are treated with GZ17-6.02 and bortezomib. (**A**, **B**) ALMC1 cells were transfected with a plasmid to express LC3-GFP-RFP and co-transfected with a scrambled siRNA or with siRNA molecules to knock down the expression of ATM, AMPKα, ULK1, Beclin1 or ATG5. Twenty-four h later, cells were treated with vehicle control, GZ17-6.02 (curcumin 2 μM, final), bortezomib (10 nM) or the drugs in combination for 4 h and 8 h. At each time point, the mean number of autophagosomes (GFP+ RFP+) and autolysosomes (RFP+) per cell were determined randomly in >100 cells. (n = 3 +/− SD). $^{*}p < 0.05$ less than corresponding value at 4 h; $^{**}p < 0.05$ less than corresponding values in siATM and siAMPK transfected cells; $^{\#}p < 0.05$ greater than corresponding value at 4 h; $^{\dagger}p < 0.05$ less than corresponding values in siATM and siAMPK transfected cells. (**C**) ALMC1 cells were transfected with a scrambled siRNA or with siRNA molecules to knock down the expression of ATM, AMPKα, ULK1, Beclin1 or ATG5. Twenty-four h later, cells were treated with vehicle control, GZ17-6.02 (curcumin 2 μM, final), bortezomib (10 nM) or the drugs in combination for 24 h. Twenty-four h later, cells were isolated, and viability determined via trypan blue exclusion assays (n = 3 +/− SD). $^{*}p < 0.05$ less than corresponding value in siSCR cells; $^{\dagger}p < 0.05$ less than corresponding values in siATM and siAMPK transfected cells.

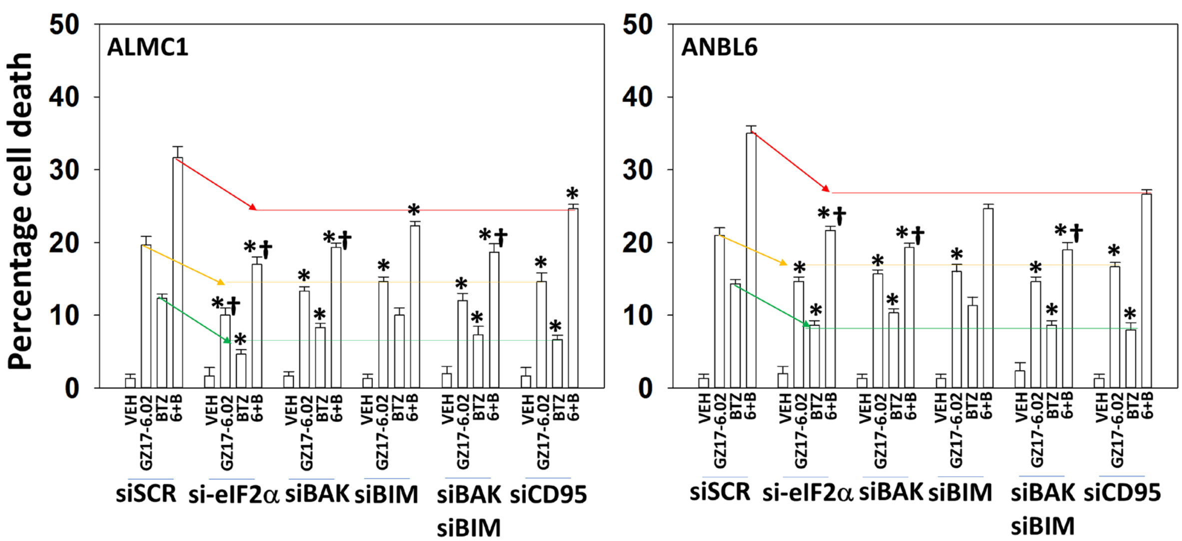

Figure 7: ER stress signaling plays an important role in mediating GZ17-6.02/bortezomib lethality. ALMC1 and ANBL6 cells were transfected with scrambled siRNA or with siRNA molecules to knock down eIF2α, BAK, BIM or CD95. After 24 h, cells were treated with vehicle control, GZ17-6.02 (2 μM curcumin, final), bortezomib (10 nM) or the drugs in combination for 24 h. Twenty-four h later, cells were isolated, and viability determined via trypan blue exclusion assays (n = 3 +/− SD). $^{*}p < 0.05$ less than corresponding value in siSCR cells; $^{\dagger}p < 0.05$ less than corresponding values in siCD95 transfected cells.

A

4h

ALMC1

	VEH	602	BTZ	602+B
H3K9ac	100	108	104	116#
H3K27ac	100	110	105	119#
H3K4ac	100	105	101	108
Histone H3	100	100	100	100

	VEH	602	BTZ	602+B
DM-K4	100	104	102	107
M-K9	100	108	101	109
M-K36	100	96	100	93
DM-K27	100	101	101	108
M-K79	100	99	98	94
Histone H3	100	100	99	100

ANBL6

	VEH	602	BTZ	602+B
H3K9ac	100	113#	108	117#
H3K27ac	100	118#	109	118#
H3K4ac	100	106	102	109
Histone H3	100	100	99	100

	VEH	602	BTZ	602+B
DM-K4	100	105	106	108
M-K9	100	102	99	104
M-K36	100	99	100	95
DM-K27	100	102	100	101
M-K79	100	98	100	95
Histone H3	100	100	100	101

24h

ALMC1

	VEH	602	BTZ	602+B
H3K9ac	100	113#	108	117#
H3K27ac	100	111	103	115#
H3K4ac	100	107	104	109
Histone H3	100	100	100	101

	VEH	602	BTZ	602+B
DM-K4	100	112	105	117#
M-K9	100	91	90	84*
M-K36	100	95	100	87*
DM-K27	100	110	105	117#
M-K79	100	91	88	80*
Histone H3	100	100	100	100

ANBL6

	VEH	602	BTZ	602+B
H3K9ac	100	108	102	116#
H3K27ac	100	109	103	120#
H3K4ac	100	107	100	109
Histone H3	100	99	100	100

	VEH	602	BTZ	602+B
DM-K4	100	110	109	116#
M-K9	100	99	96	95
M-K36	100	94	98	83*
DM-K27	100	103	97	103
M-K79	100	93	96	84*
Histone H3	100	100	100	100

B

24h + 24h

ALMC1

	VEH	602	BTZ	602+B
H3K9ac	100	105	102	114#
H3K27ac	100	108	102	115#
H3K4ac	100	104	102	107
Histone H3	100	99	99	99

	VEH	602	BTZ	602+B
DM-K4	100	108	105	113#
M-K9	100	98	98	93
M-K36	100	99	100	100
DM-K27	100	110	107	114#
M-K79	100	97	96	91
Histone H3	100	100	100	100

ANBL6

	VEH	602	BTZ	602+B
H3K9ac	100	111	108	115#
H3K27ac	100	113#	107	118#
H3K4ac	100	104	100	105
Histone H3	100	100	99	99

	VEH	602	BTZ	602+B
DM-K4	100	107	107	108
M-K9	100	101	101	93
M-K36	100	97	103	91
DM-K27	100	101	100	102
M-K79	100	99	100	97
Histone H3	100	100	100	100

48h

ALMC1

	VEH	602	BTZ	602+B
H3K9ac	100	110	104	117#
H3K27ac	100	108	100	114#
H3K4ac	100	114#	107	114#
Histone H3	100	101	100	101

	VEH	602	BTZ	602+B
DM-K4	100	109	100	114#
M-K9	100	93	92	85*
M-K36	100	94	100	92
DM-K27	100	110	102	116#
M-K79	100	93	98	87*
Histone H3	100	100	99	100

ANBL6

	VEH	602	BTZ	602+B
H3K9ac	100	114#	108	115#
H3K27ac	100	117#	106	123#
H3K4ac	100	103	99	106
Histone H3	100	99	100	100

	VEH	602	BTZ	602+B
DM-K4	100	109	107	114#
M-K9	100	98	98	96
M-K36	100	91	97	86*
DM-K27	100	109	103	115#
M-K79	100	93	95	84*
Histone H3	100	100	100	100

Figure 8: (**A**) GZ17-6.02 and bortezomib regulate histone H3 acetylation and methylation in multiple myeloma cells. ALMC1 and ANBL6 cells were treated with vehicle control, GZ17-6.02 (2 µM, curcumin final), bortezomib (10 nM) or the drugs in combination for 4 h. Cells were centrifuged and fixed *in situ*, permeabilized, stained with the indicated validated primary antibodies and imaged with secondary antibodies carrying red- and green-fluorescent tags. The staining intensity of at least 100 cells per well/condition is determined in three separate studies. The data are the normalized amount of fluorescence set at 100% comparing intensity values for vehicle control ($n = 3$ +/− SD). $^{\#}p < 0.05$ greater than vehicle control; $^{*}p < 0.05$ less than vehicle control. Tabular data are presented as a heat-map (Microsoft Excel: conditional formatting, color scales: green, yellow, red). Green indicates greater levels and red indicates lower levels of staining. (**B**) GZ17-6.02 and bortezomib regulate histone H3 acetylation and methylation in multiple myeloma cells. ALMC1 and ANBL6 cells were treated with vehicle control, GZ17-6.02 (2 µM, curcumin final), bortezomib (10 nM) or the drugs in combination for 4 h. Cells were centrifuged and fixed *in situ*, permeabilized, stained with the indicated validated primary antibodies and imaged with secondary antibodies carrying red- and green-fluorescent tags. The staining intensity of at least 100 cells per well/condition is determined in three separate studies. The data are the normalized amount of fluorescence set at 100% comparing intensity values for vehicle control ($n = 3$ +/− SD). $^{\#}p < 0.05$ greater than vehicle control; $^{*}p < 0.05$ less than vehicle control. Tabular data are presented as a heat-map (Microsoft Excel: conditional formatting, color scales: green, yellow, red). Green indicates greater levels and red indicates lower levels of staining.

A

ALMC1

	siSCR	siHDAC1/2/3
ATM	100	99
P-ATM S1981	100	115 #
AMPKα	100	98
P-AMPKα T172	100	117 #
mTOR	100	99
P-mTOR S2448	100	87 *
P-mTOR S2481	100	93
ULK1	100	99
P-ULK1 S757	100	86 *
P-ULK1 S317	100	107
eIF2α	100	100
P-eIF2α S51	100	106
PERK	100	100
P-PERK T980	100	108

	siSCR	siHDAC1/2/3
AKT	100	99
P-AKT T308	100	90
STAT3	100	99
P-STAT3 Y705	100	96
STAT5	100	99
P-STAT5 Y694	100	97
Beclin1	100	103
ATG5	100	97
ATG13	100	101
P-ATG13 S318	100	113 #
GRP78	100	103
CHOP	100	101
PP1	100	102

	siSCR	siHDAC1/2/3
NFκB	100	99
P-NFκB S536	100	87 *
c-SRC	100	100
P-SRC Y416	100	87 *
P-SRC Y527	100	103
c-MET	100	99
P-c-MET	100	98
CD95	100	114 #
FAS-L	100	100
JAK2	100	100
P-JAK2	100	95
c-KIT	100	100
P-c-KIT	100	98
p70 S6K	100	99
P-p70 S6K T389	100	91
JNK1/2	100	100
P-JNK1/2	100	83 *
p38	100	100
P-p38	100	99
P-ERK1/2	100	101
ERK1/2	100	94

B

	siSCR	siHDAC1/2/3
HDAC1	100	21 *
HDAC2	100	24 *
HDAC3	100	23 *
HDAC4	100	99
HDAC5	100	99
HDAC6	100	99
HDAC7	100	99
HDAC8	100	100
HDAC9	100	100
HDAC10	100	99
HDAC11	100	101
ERK2	100	99

	siSCR	siHDAC1/2/3	
LATS1/2	100	99	
P-LATS T1097	100	114 #	
P-LATS S909	100	116 #	
YAP	100	92	
P-YAP S109	100	106	115 #
P-YAP S127	100	119	129 #
P-YAP S397	100	110	120 #
TAZ	100	100	
P-TAZ S89	100	117 #	
ERK2	100	100	

	siSCR	siHDAC1/2/3
PD-L1	100	98
PD-L2	100	99
MHCA	100	109
ODC	100	101
IDO1	100	100
p38 MAPK	100	100
P-p38	100	100
BCL-XL	100	87 *
MCL1	100	94
BAX	100	99
BAK	100	113 #
BIM	100	107
FLIP-s	100	99
ERK2	100	100

Figure 9: (**A**) Knock down of HDACs1/2/3 regulates signaling in ALMC1 cells in a fashion similar to that of GZ17-6.02. Cells were transfected with a scrambled siRNA or with siRNAs combined to knock down the expression of HDACs1/2/3. After 12 h cells were centrifuged and fixed *in situ*, permeabilized, stained with the indicated validated primary antibodies and imaged with secondary antibodies carrying red- and green-fluorescent tags. The staining intensity of at least 100 cells per well/condition is determined in three separate studies. The data are the normalized amount of fluorescence set at 100% comparing intensity values for vehicle control ($n = 3$ +/− SD). $^{\#}p < 0.05$ greater than vehicle control; $^{*}p < 0.05$ less than vehicle control. Tabular data are presented as a heat-map (Microsoft Excel: conditional formatting, color scales: green, yellow, red). Green indicates greater levels and red indicates lower levels of staining. (**B**) Knock down of HDACs1/2/3 regulates signaling in ALMC1 cells in a fashion similar to that of GZ17-6.02. Cells were transfected with a scrambled siRNA or with siRNAs combined to knock down the expression of HDACs1/2/3. After 12 h cells were centrifuged and fixed *in situ*, permeabilized, stained with the indicated validated primary antibodies and imaged with secondary antibodies carrying red- and green-fluorescent tags. The staining intensity of at least 100 cells per well/condition is determined in three separate studies. The data are the normalized amount of fluorescence set at 100% comparing intensity values for vehicle control ($n = 3$ +/− SD). $^{\#}p < 0.05$ greater than vehicle control; $^{*}p < 0.05$ less than vehicle control. Tabular data are presented as a heat-map (Microsoft Excel: conditional formatting, color scales: green, yellow, red). Green indicates greater levels and red indicates lower levels of staining.

A

ANBL6

	siSCR	siHDAC1/2/3		siSCR	siHDAC1/2/3		siSCR	siHDAC1/2/3
ATM	100	100	AKT	100	101	NFκB	100	100
P-ATM S1981	100	119#	P-AKT T308	100	94	P-NFκB S536	100	85*
AMPKα	100	100	STAT3	100	100	c-SRC	100	100
P-AMPKα T172	100	116#	P-STAT3 Y705	100	98	P-SRC Y416	100	100
mTOR	100	101	STAT5	100	100	P-SRC Y527	100	105
P-mTOR S2448	100	77*	P-STAT5 Y694	100	95	c-MET	100	100
P-mTOR S2481	100	90	Beclin1	100	96	P-c-MET	100	101
ULK1	100	100	ATG5	100	98	CD95	100	106
P-ULK1 S757	100	86*	ATG13	100	101	FAS-L	100	106
P-ULK1 S317	100	113#	P-ATG13 S318	100	117#	JAK2	100	100
eIF2α	100	99	GRP78	100	101	P-JAK2	100	95
P-eIF2α S51	100	116#	CHOP	100	99	c-KIT	100	101
PERK	100	99	PP1	100	101	P-c-KIT	100	95
P-PERK T980	100	117#				p70 S6K	100	100
						P-p70 S6K T389	100	87*
						JNK1/2	100	99
						P-JNK1/2	100	96
						p38	100	100
						P-p38	100	99
						P-ERK1/2	100	97
						ERK1/2	100	99

B

	siSCR	siHDAC1/2/3
HDAC1	100	37*
HDAC2	100	42*
HDAC3	100	39*
HDAC4	100	101
HDAC5	100	98
HDAC6	100	83*
HDAC7	100	100
HDAC8	100	100
HDAC9	100	99
HDAC10	100	99
HDAC11	100	100
ERK2	100	100

	siSCR	siHDAC1/2/3
LATS1/2	100	99
P-LATS T1097	100	104
P-LATS S909	100	103
YAP	100	100
P-YAP S109	100	102
P-YAP S127	100	118#
P-YAP S397	100	114#
TAZ	100	100
P-TAZ S89	100	109
ERK2	100	100

	siSCR	siHDAC1/2/3
PD-L1	100	94
PD-L2	100	98
MHCA	100	108
ODC	100	100
IDO1	100	101
p38 MAPK	100	100
P-p38	100	100
BCL-XL	100	86*
MCL1	100	85*
BAX	100	99
BAK	100	117#
BIM	100	101
FLIP-s	100	100
ERK2	100	100

Figure 10: (**A**) Knock down of HDACs1/2/3 regulates signaling in ANBL6 cells in a fashion similar to that of GZ17-6.02. Cells were transfected with a scrambled siRNA or with siRNAs combined to knock down the expression of HDACs1/2/3. After 12 h cells were centrifuged and fixed *in situ*, permeabilized, stained with the indicated validated primary antibodies and imaged with secondary antibodies carrying red- and green-fluorescent tags. The staining intensity of at least 100 cells per well/condition is determined in three separate studies. The data are the normalized amount of fluorescence set at 100% comparing intensity values for vehicle control ($n = 3$ +/− SD). $^{\#}p <$ 0.05 greater than vehicle control; $^{*}p < 0.05$ less than vehicle control. Tabular data are presented as a heat-map (Microsoft Excel: conditional formatting, color scales: green, yellow, red). Green indicates greater levels and red indicates lower levels of staining. (**B**) Knock down of HDACs1/2/3 regulates signaling in ANBL6 cells in a fashion similar to that of GZ17-6.02. Cells were transfected with a scrambled siRNA or with siRNAs combined to knock down the expression of HDACs1/2/3. After 12 h cells were centrifuged and fixed *in situ*, permeabilized, stained with the indicated validated primary antibodies and imaged with secondary antibodies carrying red- and green-fluorescent tags. The staining intensity of at least 100 cells per well/condition is determined in three separate studies. The data are the normalized amount of fluorescence set at 100% comparing intensity values for vehicle control ($n = 3$ +/− SD). $^{\#}p < 0.05$ greater than vehicle control; $^{*}p < 0.05$ less than vehicle control. Tabular data are presented as a heat-map (Microsoft Excel: conditional formatting, color scales: green, yellow, red). Green indicates greater levels and red indicates lower levels of staining.

Based on the large reductions in HDAC1/2/3 expression caused by GZ17-6.02 as a single agent and more so when combined with bortezomib, we determined whether the acetylation and methylation of lysine residues within histone H3 were altered. The acetylation of histone H3 at lysine 9 and at lysine 27 was enhanced within 4 h by GZ17-6.02 as a single agent and this persisted for 48 h; even in cells cultured in the absence of the drug for 24 h, acetylation at these sites was maintained. In contrast, no changes in histone H3 methylation were observed after 4 h of treatment, and after 24 h, in both cell lines tested, the di-methylation of lysine 4 was elevated only by the drug combination and the methylation of lysine 36 and lysine 79 reduced, again only by the drug combination. After 48 h, in both lines, the di-methylation of lysine 4 remained high as was di-methylation of lysine 27. The methylation of lysine 79 in both lines remained lower.

Acetylation and methylation of histone H3 has been linked in multiple tumor cell types to the regulation of transcription, and GZ17-6.02 has been linked to the regulation of super-enhancer elements [37]. Mithraprabhu et al. and Yuan et al. both demonstrated that MM cells are sensitive in the laboratory and in patients to histone deacetylase inhibitors [38, 39]. Elevated histone H3 lysine 27 acetylation is indicative of gene activation in multiple myeloma cells and was associated with poorer patient survival [40]. Silencing of the transcription factor ELK1 was associated with decreased histone H3 lysine 9 acetylation, increased lysine 9 methylation and reduced expression of the pluripotency gene Oct4 [41]. Changes in histone methylation were delayed secondary events compared to alterations in acetylation. Di- and tri-methylation of lysine 4 are markers of transcriptional activation and we observed prolonged di-methylation of lysine 4 after 24 h of GZ17-6.02 and bortezomib exposure [42]. Reduced lysine 79 methylation would be predicted to correlate with reduced transcription [43, 44]. Increased K79 methylation has also been linked to UV-induced recombination repair and cell cycle checkpoint activation, which potentially links our observation that knock down of HDAC proteins activated ATM [45].

GZ17-6.02 as a single agent and when combined with bortezomib enhanced phosphorylation of threonine 3 in both lines and this was maintained for 48 h. Phosphorylation of T3 has been linked to chromosome segregation, chromosome methylation and signaling by the Aroura B kinase/protein phosphatase 1 complex [46–49]. For example, the demethylase Dnmt3a interacts with the H3 histone tail and binding can be disrupted by di- and trimethylation of K4, acetylation of K4 and by phosphorylation of T3. In addition to these findings is that Aurora B is the catalytic 'kinase' subunit which coordinates mitosis. In prometaphase, the Aroura B kinase/protein phosphatase 1/Haspin complex is enriched at centromeres and controls spindle checkpoint and kinetochore-microtubule interactions. Future studies will need to address the relevance of the alterations in acetylation, methylation, and phosphorylation to the MM biology of GZ17-6.02.

Knock down of eIF2α significantly reduced the lethality of GZ17-6.02 and of bortezomib as single agents, and more so when cells were treated with the drug combination. This correlates with our findings from both MM lines examining the phosphorylation of PERK and eIF2α where in general, it was the drug combination that was required to generate a significant endoplasmic reticulum response [15–23]. In MM the PERK-eIF2α-ATF4-CHOP ER stress response has been linked by many groups to elevated tumor cell killing [50–52]. As noted earlier, many groups have also linked macroautophagy to proteasome inhibitor resistance, including autophagy stimulated by ER stress [53]. Our data demonstrated that autophagosome formation and MM cell killing by the drug combination was most effectively reduced by knocking down the expression of ULK1, Beclin1 or ATG5, strongly arguing that macroautophagy played a key role in tumor cell execution. As a single agent and as previously observed in solid tumor cells, GZ17-6.02 enhanced macroautophagy which was essential for tumor cell killing. However, we did not expect cell killing by bortezomib as a single agent to also be reduced by knock down of ULK1, Beclin1 or ATG5. Reasons for the difference between our data and other groups may be linked to the relatively low concentrations of bortezomib used in our studies, and that our genetic manipulations were transient rather than stable knock downs.

GZ17-6.02 and bortezomib activated LATS1/2 and increased the phosphorylation of YAP and TAZ in the Hippo pathway; YAP and TAZ phosphorylation causes their nuclear exit and prevents them from acting as co-transcription factors with TEADS proteins in the nucleus [54–61]. In solid tumor cell types, nuclear-localized YAP and TAZ play key roles in promoting tumor cell growth, metastatic spread, and resistance to chemotherapy. In MM cells, the literature argues both for YAP and TAZ acting under some circumstances as tumor promoters and situationally acting as tumor suppressors. YAP can associate with both acetylases and methylases to alter chromatin structure and transcription. Studies beyond the present manuscript will be required to understand the relevance of the Hippo pathway to the biology of GZ17-6.02 in MM cells.

MATERIALS AND METHODS

Materials

The ALMC1, ANBL6 and U266 multiple myeloma cell lines were purchased from the ATCC (Bethesda, MD, USA). Bortezomib and carfilzomib were purchased from Selleckchem (Houston, TX, USA). All Materials were obtained as described in the references [14–23]. Trypsin-EDTA, DMEM, RPMI, penicillin-streptomycin were purchased from GIBCOBRL (GIBCOBRL Life Technologies, Grand Island, NY, USA). Other reagents and performance of experimental procedures were as described [14–23]. Antibodies were purchased from Cell Signaling Technology (Danvers, MA, USA); Abgent (San Diego, CA, USA); Novus Biologicals (Centennial, CO, USA); Abcam (Cambridge, UK); and Santa Cruz Biotechnology (Dallas, TX, USA). Specific multiple independent siRNAs to knock down the expression of CD95, Beclin1, ATG5, AMPKα_1, ATM, BIM, BAX, BAK, BID and eIF2α, and scramble control, were purchased from Qiagen (Hilden, Germany) and Thermo Fisher (Waltham, MA, USA). Control studies were presented in prior manuscripts showing on-target specificity of our siRNAs, primary antibodies, and our phospho-specific antibodies to detect both total protein levels and phosphorylated levels of proteins [14–23] (Supplementary Figure 8).

Methods

All bench-side Methods used in this manuscript have been previously performed and described in the peer-reviewed references [14–23].

Assessments of protein expression and protein phosphorylation [14–23]

At various time-points after the initiation of drug exposure, cells in 96-well plates are fixed in place using paraformaldehyde and using Triton X100 for permeabilization. Standard immunofluorescent blocking procedures are employed, followed by incubation of different wells with a variety of validated primary antibodies and subsequently validated fluorescent-tagged secondary antibodies are added to each well. Assessments of staining intensity were made using a Hermes wide field microscope (Idea Biotechnology, Rehovot, Israel) using its internal software. Tabular data are presented as a heat-map (Microsoft Excel: conditional formatting, color scales: green, yellow, red). Green indicates greater levels and red indicates lower levels of staining.

Detection of cell death by trypan blue assay [14–23]

Cells were treated with vehicle control or with drugs alone or in combination for 24 h. At the indicated time points cells were harvested by trypsinization and centrifugation. Cell pellets were resuspended in PBS and mixed with trypan blue agent. Viability was determined microscopically using a hemocytometer. Five hundred cells randomly chosen from the four fields of the hemocytometer were counted and the number of dead cells was counted and expressed as a percentage of the total number of cells counted.

Transfection of cells with siRNA [14–23]

Cells were plated and 24 h after plating, transfected. A plasmid to express LC3-GFP-RFP was used throughout the study (Addgene, Waltham, MA). For siRNA transfection, 10 nM of the annealed siRNA or the negative control (a “scrambled” sequence with no significant homology to any known gene sequences from mouse, rat, or human cell lines) were used.

Assessments of autophagosome and autolysosome levels [14–23]

Cells were transfected with a plasmid to express LC3-GFP-RFP (Addgene, Watertown MA). Twenty-four hours after transfection, cells are treated with vehicle control or the drugs alone or in combination. Cells were imaged and recorded at 60X magnification 4 h and 8 h after drug exposure and the mean number of (GFP+RFP+) and (RFP+) punctae per cell determined from >100 randomly selected cells per condition.

Data analysis

Comparison of the effects of various treatments was using one-way ANOVA for normalcy followed by a two tailed Student’s *t*-test with multiple comparisons. Differences with a *p*-value of < 0.05 were considered statistically significant. Experiments are the means of multiple individual data points per experiment from 3 independent experiments (± SD).

Abbreviations

ERK: extracellular regulated kinase; PI3K: phosphatidyl inositol 3 kinase; ca: constitutively active; dn: dominant negative; ER: endoplasmic reticulum; AMPK: AMP-dependent protein kinase; mTOR: mammalian target of rapamycin; JAK: Janus Kinase; STAT: Signal Transducers and Activators of Transcription; MAPK: mitogen activated protein kinase; PTEN: phosphatase and tensin homologue on chromosome ten; ROS: reactive oxygen species; CMV: empty vector plasmid; si: small interfering; SCR: scrambled; VEH: vehicle; 602: GZ17-6.02; BTZ: bortezomib; MHCA: major histocompatibility class A.

Author contributions

LB and JLR performed the studies. PD directed the studies. CW collaborated with PD to develop the studies and critically read the final manuscript. We thank Dr. Roy

Sabo (VCU, Biostatistics), for biostatistical assistance during these studies.

CONFLICTS OF INTEREST

PD has received funding support from Genzada Pharmaceuticals Inc. for these studies. Dr. West is a paid officer of the company. Dr. Dent is a Consultant and Key Scientific advisor to the company. PD and CW thank Dr. Daniel Von Hoff, a consultant and key scientific advisor for Genzada Pharmaceuticals, for expert guidance during performance of these studies and for editing the manuscript.

FUNDING

PD acknowledges funding Genzada Pharmaceuticals USA, Inc.

REFERENCES

1. Albagoush SA, Shumway C, Azevedo AM. Multiple Myeloma. In: StatPearls. Treasure Island (FL): StatPearls Publishing; 2024. [PubMed]
2. Becker N. Epidemiology of multiple myeloma. Recent Results Cancer Res. 2011; 183:25–35. https://doi.org/10.1007/978-3-540-85772-3_2. [PubMed]
3. Alexander DD, Mink PJ, Adami HO, Cole P, Mandel JS, Oken MM, Trichopoulos D. Multiple myeloma: a review of the epidemiologic literature. Int J Cancer. 2007 (Suppl 12); 120:40–61. https://doi.org/10.1002/ijc.22718. [PubMed]
4. Leng Y, Hu X, Li L, Nkwocha J, Satta T, Sharma K, Kmeiciak M, Zhou H, Zhang Z, Zhou L, Chen W, Grant S. Mechanisms underlying synergism between circularized tumor necrosis factor-related apoptosis inducing ligand and bortezomib in bortezomib-sensitive or -resistant myeloma cells. Hematol Oncol. 2022; 40:999–1008. https://doi.org/10.1002/hon.3045. [PubMed]
5. Richardson PG, Hideshima T, Anderson KC. Bortezomib (PS-341): a novel, first-in-class proteasome inhibitor for the treatment of multiple myeloma and other cancers. Cancer Control. 2003; 10:361–69. https://doi.org/10.1177/107327480301000502. [PubMed]
6. Herndon TM, Deisseroth A, Kaminskas E, Kane RC, Koti KM, Rothmann MD, Habtemariam B, Bullock J, Bray JD, Hawes J, Palmby TR, Jee J, Adams W, et al. U.s. Food and Drug Administration approval: carfilzomib for the treatment of multiple myeloma. Clin Cancer Res. 2013; 19:4559–63. https://doi.org/10.1158/1078-0432.CCR-13-0755. [PubMed]
7. Sadek NL, Costa BA, Nath K, Mailankody S. CAR T-Cell Therapy for Multiple Myeloma: A Clinical Practice-Oriented Review. Clin Pharmacol Ther. 2023; 114:1184–95. https://doi.org/10.1002/cpt.3057. [PubMed]
8. Scheller L, Tebuka E, Rambau PF, Einsele H, Hudecek M, Prommersberger SR, Danhof S. BCMA CAR-T cells in multiple myeloma-ready for take-off? Leuk Lymphoma. 2024; 65:143–57. https://doi.org/10.1080/10428194.2023.2276676. [PubMed]
9. Fazio M, Del Fabro V, Parrinello NL, Allegra A, Markovic U, Botta C, Accardi F, Vincelli ID, Leotta S, Elia F, Esposito B, Garibaldi B, Sapuppo G, et al. Multiple Myeloma in 2023 Ways: From Trials to Real Life. Curr Oncol. 2023; 30:9710–33. https://doi.org/10.3390/curroncol30110705. [PubMed]
10. Anderson LD Jr, Dhakal B, Jain T, Oluwole OO, Shah GL, Sidana S, Perales MA, Pasquini MC. Chimeric Antigen Receptor T Cell Therapy for Myeloma: Where Are We Now and What Is Needed to Move Chimeric Antigen Receptor T Cells Forward to Earlier Lines of Therapy? Expert Panel Opinion from the American Society for Transplantation and Cellular Therapy. Transplant Cell Ther. 2024; 30:17–37. https://doi.org/10.1016/j.jtct.2023.10.022. [PubMed]
11. Vishwakarma V, New J, Kumar D, Snyder V, Arnold L, Nissen E, Hu Q, Cheng N, Miller D, Thomas AR, Shnayder Y, Kakarala K, Tsue TT, et al. Potent Antitumor Effects of a Combination of Three Nutraceutical Compounds. Sci Rep. 2018; 8:12163. https://doi.org/10.1038/s41598-018-29683-1. [PubMed]
12. Hsu KY, Ho CT, Pan MH. The therapeutic potential of curcumin and its related substances in turmeric: From raw material selection to application strategies. J Food Drug Anal. 2023; 31:194–211. https://doi.org/10.38212/2224-6614.3454. [PubMed]
13. de Waure C, Bertola C, Baccarini G, Chiavarini M, Mancuso C. Exploring the Contribution of Curcumin to Cancer Therapy: A Systematic Review of Randomized Controlled Trials. Pharmaceutics. 2023; 15:1275. https://doi.org/10.3390/pharmaceutics15041275. [PubMed]
14. Dent P, Booth L, Roberts JL, Poklepovic A, Hancock JF. (Curcumin+sildenafil) enhances the efficacy of 5FU and anti-PD1 therapies in vivo. J Cell Physiol. 2020; 235:6862–74. https://doi.org/10.1002/jcp.29580. [PubMed]
15. Booth L, Roberts JL, West C, Von Hoff D, Dent P. GZ17-6.02 initiates DNA damage causing autophagosome-dependent HDAC degradation resulting in enhanced anti-PD1 checkpoint inhibitory antibody efficacy. J Cell Physiol. 2020; 235:8098–113. https://doi.org/10.1002/jcp.29464. [PubMed]
16. Booth L, West C, Moore RP, Von Hoff D, Dent P. GZ17-6.02 and Pemetrexed Interact to Kill Osimertinib-Resistant NSCLC Cells That Express Mutant ERBB1 Proteins. Front Oncol. 2021; 11:711043. https://doi.org/10.3389/fonc.2021.711043. [PubMed]
17. Booth L, West C, Von Hoff D, Kirkwood JM, Dent P. GZ17-6.02 Interacts With [MEK1/2 and B-RAF Inhibitors] to Kill Melanoma Cells. Front Oncol. 2021; 11:656453. https://doi.org/10.3389/fonc.2021.656453. [PubMed]

18. Booth L, West C, Moore RP, Von Hoff D, Dent P. GZ17-6.02 and palbociclib interact to kill ER+ breast cancer cells. Oncotarget. 2022; 13:92–104. https://doi.org/10.18632/oncotarget.28177. [PubMed]
19. West CE, Kwatra SG, Choi J, Von Hoff D, Booth L, Dent P. A novel plant-derived compound is synergistic with 5-fluorouracil and has increased apoptotic activity through autophagy in the treatment of actinic keratoses. J Dermatolog Treat. 2022; 33:590–91. https://doi.org/10.1080/09546634.2020.1764905. [PubMed]
20. Bordeaux ZA, Kwatra SG, Booth L, Dent P. A novel combination of isovanillin, curcumin, and harmine (GZ17-6.02) enhances cell death and alters signaling in actinic keratoses cells when compared to individual components and two-component combinations. Anticancer Drugs. 2023; 34:544–50. https://doi.org/10.1097/CAD.0000000000001425. [PubMed]
21. Booth L, Roberts JL, West C, Dent P. GZ17-6.02 kills prostate cancer cells in vitro and in vivo. Front Oncol. 2022; 12:1045459. https://doi.org/10.3389/fonc.2022.1045459. [PubMed]
22. Booth L, West C, Von Hoff D, Dent P. Mechanisms of GZ17-6.02 resistance. Anticancer Drugs. 2022; 33:415–23. https://doi.org/10.1097/CAD.0000000000001203. [PubMed]
23. Booth L, West C, Hoff DV, Dent P. GZ17-6.02 and Doxorubicin Interact to Kill Sarcoma Cells via Autophagy and Death Receptor Signaling. Front Oncol. 2020; 10:1331. https://doi.org/10.3389/fonc.2020.01331. [PubMed]
24. Ali-Shtayeh MS, Jamous RM, Salameh NM, Jamous RM, Hamadeh AM. Complementary and alternative medicine use among cancer patients in Palestine with special reference to safety-related concerns. J Ethnopharmacol. 2016; 187:104–22. https://doi.org/10.1016/j.jep.2016.04.038. [PubMed]
25. Zhang L, Zhang F, Zhang W, Chen L, Gao N, Men Y, Xu X, Jiang Y. Harmine suppresses homologous recombination repair and inhibits proliferation of hepatoma cells. Cancer Biol Ther. 2015; 16:1585–92. https://doi.org/10.1080/15384047.2015.1078021. [PubMed]
26. Ma Y, Wink M. The beta-carboline alkaloid harmine inhibits BCRP and can reverse resistance to the anticancer drugs mitoxantrone and camptothecin in breast cancer cells. Phytother Res. 2010; 24:146–49. https://doi.org/10.1002/ptr.2860. [PubMed]
27. Chang YC, Lee FW, Chen CS, Huang ST, Tsai SH, Huang SH, Lin CM. Structure-activity relationship of C6-C3 phenylpropanoids on xanthine oxidase-inhibiting and free radical-scavenging activities. Free Radic Biol Med. 2007; 43:1541–51. https://doi.org/10.1016/j.freeradbiomed.2007.08.018. [PubMed]
28. Boeira JM, Viana AF, Picada JN, Henriques JA. Genotoxic and recombinogenic activities of the two beta-carboline alkaloids harman and harmine in Saccharomyces cerevisiae. Mutat Res. 2002; 500:39–48. https://doi.org/10.1016/s0027-5107(01)00294-9. [PubMed]
29. Li S, Cheng X, Wang C. A review on traditional uses, phytochemistry, pharmacology, pharmacokinetics and toxicology of the genus Peganum. J Ethnopharmacol. 2017; 203:127–62. https://doi.org/10.1016/j.jep.2017.03.049. [PubMed]
30. Chen J, Cao W, Huang X, Chen Q, Ye S, Qu J, Liu Y, Guo X, Yao S, Zhang E, He J, Li A, Yang L, Cai Z. TRIM21 enhances bortezomib sensitivity in multiple myeloma by halting prosurvival autophagy. Blood Adv. 2023; 7:5752–70. https://doi.org/10.1182/bloodadvances.2022008241. [PubMed]
31. Zang X, Wang J, Xia Y, Li J, Chen L, Gu Y, Shen X. LncRNA MEG3 promotes the sensitivity of bortezomib by inhibiting autophagy in multiple myeloma. Leuk Res. 2022; 123:106967. https://doi.org/10.1016/j.leukres.2022.106967. [PubMed]
32. Salimi A, Schroeder KM, Schemionek-Reinders M, Vieri M, Maletzke S, Gezer D, Masouleh BK, Appelmann I. Targeting autophagy increases the efficacy of proteasome inhibitor treatment in multiple myeloma by induction of apoptosis and activation of JNK. BMC Cancer. 2022; 22:735. https://doi.org/10.1186/s12885-022-09775-y. [PubMed]
33. Nikesitch N, Rebeiro P, Ho LL, Pothula S, Wang XM, Khong T, Quek H, Spencer A, Lee CS, Roberts TL, Ling SCW. The Role of Chaperone-Mediated Autophagy in Bortezomib Resistant Multiple Myeloma. Cells. 2021; 10:3464. https://doi.org/10.3390/cells10123464. [PubMed]
34. Li H, Roy M, Liang L, Cao W, Hu B, Li Y, Xiao X, Wang H, Ye M, Sun S, Zhang B, Liu J. Deubiquitylase USP12 induces pro-survival autophagy and bortezomib resistance in multiple myeloma by stabilizing HMGB1. Oncogene. 2022; 41:1298–308. https://doi.org/10.1038/s41388-021-02167-9. [PubMed]
35. Han Q, Bai H, Xu Y, Zhou M, Zhou H, Dong X, Chen B. Solamargine induces autophagy-mediated apoptosis and enhances bortezomib activity in multiple myeloma. Clin Exp Pharmacol Physiol. 2022; 49:674–85. https://doi.org/10.1111/1440-1681.13643. [PubMed]
36. Huang X, Cao W, Yao S, Chen J, Liu Y, Qu J, Li Y, Han X, He J, Huang H, Zhang E, Cai Z. NEDD4L binds the proteasome and promotes autophagy and bortezomib sensitivity in multiple myeloma. Cell Death Dis. 2022; 13:197. https://doi.org/10.1038/s41419-022-04629-8. [PubMed]
37. Ghosh C, Paul S, Dandawate P, Gunewardena SS, Subramaniam D, West C, Anant S, Dhar A. Super-enhancers: novel target for pancreatic ductal adenocarcinoma. Oncotarget. 2019; 10:1554–71. https://doi.org/10.18632/oncotarget.26704. [PubMed]
38. Mithraprabhu S, Kalff A, Gartlan KH, Savvidou I, Khong T, Ramachandran M, Cooke RE, Bowen K, Hill GR, Reynolds J, Spencer A. Phase II trial of single-agent panobinostat

consolidation improves responses after sub-optimal transplant outcomes in multiple myeloma. Br J Haematol. 2021; 193:160–70. https://doi.org/10.1111/bjh.17080. [PubMed]

39. Yuan XG, Huang YR, Yu T, Jiang HW, Xu Y, Zhao XY. Chidamide, a histone deacetylase inhibitor, induces growth arrest and apoptosis in multiple myeloma cells in a caspase-dependent manner. Oncol Lett. 2019; 18:411–19. https://doi.org/10.3892/ol.2019.10301. [PubMed]

40. Jia Y, Zhou J, Tan TK, Chung TH, Chen Y, Chooi JY, Sanda T, Fullwood MJ, Xiong S, Toh SHM, Balan K, Wong RWJ, Lim JSL, et al. Super Enhancer-Mediated Upregulation of HJURP Promotes Growth and Survival of t(4;14)-Positive Multiple Myeloma. Cancer Res. 2022; 82:406–18. https://doi.org/10.1158/0008-5472.CAN-21-0921. [PubMed]

41. Zhao Y, Zhai Y, Fu C, Shi L, Kong X, Li Q, Yu H, An X, Zhang S, Li Z. Transcription factor ELK1 regulates the expression of histone 3 lysine 9 to affect developmental potential of porcine preimplantation embryos. Theriogenology. 2023; 206:170–80. https://doi.org/10.1016/j.theriogenology.2023.05.018. [PubMed]

42. Ohguchi Y, Ohguchi H. Diverse Functions of KDM5 in Cancer: Transcriptional Repressor or Activator? Cancers (Basel). 2022; 14:3270. https://doi.org/10.3390/cancers14133270. [PubMed]

43. Worden EJ, Hoffmann NA, Hicks CW, Wolberger C. Mechanism of Cross-talk between H2B Ubiquitination and H3 Methylation by Dot1L. Cell. 2019; 176:1490–501.e12. https://doi.org/10.1016/j.cell.2019.02.002. [PubMed]

44. Yi X, Jiang XJ, Li XY, Jiang DS. Histone methyltransferases: novel targets for tumor and developmental defects. Am J Transl Res. 2015; 7:2159–75. [PubMed]

45. Rossodivita AA, Boudoures AL, Mecoli JP, Steenkiste EM, Karl AL, Vines EM, Cole AM, Ansbro MR, Thompson JS. Histone H3 K79 methylation states play distinct roles in UV-induced sister chromatid exchange and cell cycle checkpoint arrest in Saccharomyces cerevisiae. Nucleic Acids Res. 2014; 42:6286–99. https://doi.org/10.1093/nar/gku242. [PubMed]

46. Xie J, Wooten M, Tran V, Chen BC, Pozmanter C, Simbolon C, Betzig E, Chen X. Histone H3 Threonine Phosphorylation Regulates Asymmetric Histone Inheritance in the Drosophila Male Germline. Cell. 2015; 163:920–33. https://doi.org/10.1016/j.cell.2015.10.002. [PubMed]

47. Qian J, Lesage B, Beullens M, Van Eynde A, Bollen M. PP1/Repo-man dephosphorylates mitotic histone H3 at T3 and regulates chromosomal aurora B targeting. Curr Biol. 2011; 21:766–73. https://doi.org/10.1016/j.cub.2011.03.047. [PubMed]

48. Zhang Y, Jurkowska R, Soeroes S, Rajavelu A, Dhayalan A, Bock I, Rathert P, Brandt O, Reinhardt R, Fischle W, Jeltsch A. Chromatin methylation activity of Dnmt3a and Dnmt3a/3L is guided by interaction of the ADD domain with the histone H3 tail. Nucleic Acids Res. 2010; 38:4246–53. https://doi.org/10.1093/nar/gkq147. [PubMed]

49. Qian J, Beullens M, Lesage B, Bollen M. Aurora B defines its own chromosomal targeting by opposing the recruitment of the phosphatase scaffold Repo-Man. Curr Biol. 2013; 23:1136–43. https://doi.org/10.1016/j.cub.2013.05.017. [PubMed]

50. Bagratuni T, Sklirou AD, Kastritis E, Liacos CI, Spilioti C, Eleutherakis-Papaiakovou E, Kanellias N, Gavriatopoulou M, Terpos E, Trougakos IP, Dimopoulos MA. Toll-Like Receptor 4 Activation Promotes Multiple Myeloma Cell Growth and Survival Via Suppression of The Endoplasmic Reticulum Stress Factor Chop. Sci Rep. 2019; 9:3245. https://doi.org/10.1038/s41598-019-39672-7. [PubMed]

51. Gomez-Bougie P, Halliez M, Moreau P, Pellat-Deceunynck C, Amiot M. Repression of Mcl-1 and disruption of the Mcl-1/Bak interaction in myeloma cells couple ER stress to mitochondrial apoptosis. Cancer Lett. 2016; 383:204–11. https://doi.org/10.1016/j.canlet.2016.09.030. [PubMed]

52. Zhong Y, Zhang Y, Wang P, Gao H, Xu C, Li H. V8 induces apoptosis and the endoplasmic reticulum stress response in human multiple myeloma RPMI 8226 cells via the PERK-eIF2α-ATF4 signaling pathway. Oncol Lett. 2016; 12:2702–9. https://doi.org/10.3892/ol.2016.5005. [PubMed]

53. Milan E, Perini T, Resnati M, Orfanelli U, Oliva L, Raimondi A, Cascio P, Bachi A, Marcatti M, Ciceri F, Cenci S. A plastic SQSTM1/p62-dependent autophagic reserve maintains proteostasis and determines proteasome inhibitor susceptibility in multiple myeloma cells. Autophagy. 2015; 11:1161–78. https://doi.org/10.1080/15548627.2015.1052928. [PubMed]

54. Abegunde SO, Grieve S, Alfarra H, Reiman T. MST1 downregulates TAZ tumor suppressor protein in multiple myeloma and is a potential therapeutic target. Exp Hematol. 2023; 123:34–45. https://doi.org/10.1016/j.exphem.2023.04.004. [PubMed]

55. Allegra A, Pioggia G, Innao V, Musolino C, Gangemi S. New Insights into YES-Associated Protein Signaling Pathways in Hematological Malignancies: Diagnostic and Therapeutic Challenges. Cancers (Basel). 2021; 13:1981. https://doi.org/10.3390/cancers13081981. [PubMed]

56. Hillmer RE, Link BA. The Roles of Hippo Signaling Transducers Yap and Taz in Chromatin Remodeling. Cells. 2019; 8:502. https://doi.org/10.3390/cells8050502. [PubMed]

57. Fan S, Price T, Huang W, Plue M, Warren J, Sundaramoorthy P, Paul B, Feinberg D, MacIver N, Chao N, Sipkins D, Kang Y. PINK1-Dependent Mitophagy Regulates the Migration and Homing of Multiple Myeloma Cells via the MOB1B-Mediated Hippo-YAP/TAZ Pathway. Adv Sci (Weinh). 2020; 7:1900860. https://doi.org/10.1002/advs.201900860. [PubMed]

58. Qing Y, Yin F, Wang W, Zheng Y, Guo P, Schozer F, Deng H, Pan D. The Hippo effector Yorkie activates transcription by interacting with a histone

methyltransferase complex through Ncoa6. Elife. 2014; 3:e02564. https://doi.org/10.7554/eLife.02564. [PubMed]

59. Oh H, Slattery M, Ma L, White KP, Mann RS, Irvine KD. Yorkie promotes transcription by recruiting a histone methyltransferase complex. Cell Rep. 2014; 8:449–59. https://doi.org/10.1016/j.celrep.2014.06.017. [PubMed]

60. Pan Z, Tian Y, Cao C, Niu G. The Emerging Role of YAP/TAZ in Tumor Immunity. Mol Cancer Res. 2019; 17:1777–86. https://doi.org/10.1158/1541-7786.MCR-19-0375. [PubMed]

61. Yu M, Peng Z, Qin M, Liu Y, Wang J, Zhang C, Lin J, Dong T, Wang L, Li S, Yang Y, Xu S, Guo W, et al. Interferon-γ induces tumor resistance to anti-PD-1 immunotherapy by promoting YAP phase separation. Mol Cell. 2021; 81:1216–30.e9. https://doi.org/10.1016/j.molcel.2021.01.010. [PubMed]